### Title

Emission colour tuning through coupled N/La introduction in $Sr_2SiO_4:Eu^{2+}$




### Authors

Black, Ashley P
Denault, Kristin A
Frontera, Carlos
et al.



### Publication Date

2015

### DOI

10.1039/C5TC02437D

Peer reviewed

# Emission colour tuning through coupled N/La introduction in $Sr_2SiO_4$: $Eu^{2+}$

Ashley P. Black,[a] Kristin A. Denault,[b] Carlos Frontera,[a] Ram Seshadri,[b] Alejandro R. Goñi[a,c] and Amparo Fuertes [a,*]

The solid solution $Sr_{2-x}La_xSiO_{4-x}N_x$ (0≥x≥1), obtained by concomitant substitution of $Sr^{2+}$ by $La^{3+}$ and $O^{2-}$ by $N^{3-}$ in $Sr_2SiO_4$, has been prepared by solid state reaction at 1500 °C in $N_2/H_2$ of mixtures of SrO, $La_2O_3$, $SiO_2$ and $Si_3N_4$. Synchrotron radiation X-ray diffraction studies show a transition from the monoclinic $P2_1/n$ symmetry of β–$Sr_2SiO_4$ to orthorhombic Pmnb α′, β-$K_2SO_4$ type phase for x≥ 0.2. The α' phase is stabilized as a consequence of the increase in bond valence of the cations induced by nitriding. The activation with $Eu^{2+}$ and $Ce^{3+}$ of $Sr_{2-x}La_xSiO_{4-x}N_x$ produces luminescent materials with broad emission bands centered up to 650 nm under excitation at 405 nm. The emission wavelengths are tuned by La/N contents in a wide range with emission colours changing from yellow (x=0.2) to orange-red (x=1) for $Eu^{2+}$ phosphors and from blue-green (x=0.2) to orange-yellow (x=1) in $Ce^{3+}$ samples.

## 1. Introduction

In recent years general lighting has experienced a true revolution. The traditional incandescent bulb has been phased out by many governments worldwide and has been substituted by high energy efficient devices such as compact fluorescent lamps (CFL) and white light emitting diodes (LEDs). Solid state lighting (SSL) offers advantages over alternative devices including long lifetime, high efficiency, instant start, spectral flexibility and absence of toxic elements such as mercury. Switching towards SSL is the most cost effective way to reduce energy consumption and it would suppose by itself an energy saving of 10 % of all electricity consumption in the EU.[1] The first commercial white LED produced by combining a blue light-emitting InGaN with a yellow YAG:$Ce^{3+}$ phosphor shows a relatively poor color rending index due to its lack of emission in the red region of visible spectrum.[2] Numerous efforts have been directed towards the design of an efficient blue to orange/red phosphor converter.[3, 4, 5, 6, 7] Crystal site engineering offers the possibility to tune the luminescent color of a phosphor by changing the coordination environment of the activator. [8] Wide band, red luminescent emissions can be generated with $Eu^{2+}$ or $Ce^{3+}$ doping in sites with a strong crystal field splitting and large covalency of bonding.

Nitrogen and oxygen show similar crystal chemistry features and may substitute for each other in the same crystallographic sites. Nitrogen is less electronegative and more polarizable than oxygen and its introduction in an oxidic compound increases the covalent character of the bonds with the cations. The interelectronic repulsion decreases (the nephelauxetic effect increases), and the higher charge of nitride induces a larger crystal field splitting. [9] As a result the d orbitals of $Eu^{2+}$ or $Ce^{3+}$ lower in energy which leads to a red shift of the $4f^{n-1}5d^1 \rightarrow 4f^n$ emission. (Oxy)nitridosilicates have been intensively investigated as hosts for $Eu^{2+}$ or $Ce^{3+}$ phosphor components in LEDs showing long wavelengths and broad emission bands.[10, 11, 12,13, 14, 15]

The orthosilicate phosphors $M_2SiO_4$:$Eu^{2+}$ (M=Ca, Sr, Ba) show emission wavelengths from c.a. 500 nm to 600 nm under excitation with UV light from c.a. 300 to 450 nm and internal quantum efficiencies ranging from 30 % to 90 % depending on the composition and synthesis conditions.[16, 17, 18, 19 ,20, 21, 22, 23] The host compounds adopt different structures with relative stability depending on the alkaline earth cation and with increasing polymorphism as the cation size decreases. The stable polymorph of $Sr_2SiO_4$ below 85 °C is the monoclinic β phase with space group $P2_1/n$ that shows two sites for the Sr atoms with coordination numbers 10 (Sr(1)) and 9 (Sr(2)). (Figure 1a) Above this temperature it transforms into the orthorhombic α' phase, β-$K_2SO_4$ type with Pmnb space group. The mechanism of this transition is displacive; in the more stable β form the Sr(1) atoms are shifted with respect to the α' phase where they are placed at a mirror plane and are largely underbonded to the oxygen atoms (Bond valence sums (BVS) = 1.58 in α' form *vs* 1.78 in β form).[24, 25] The α' form shows an incommensurate superstructure related to the tilting of $SiO_4$ tetrahedra that improves the bond valence of Sr(1) atoms.[26] This polymorph can be stabilized at room

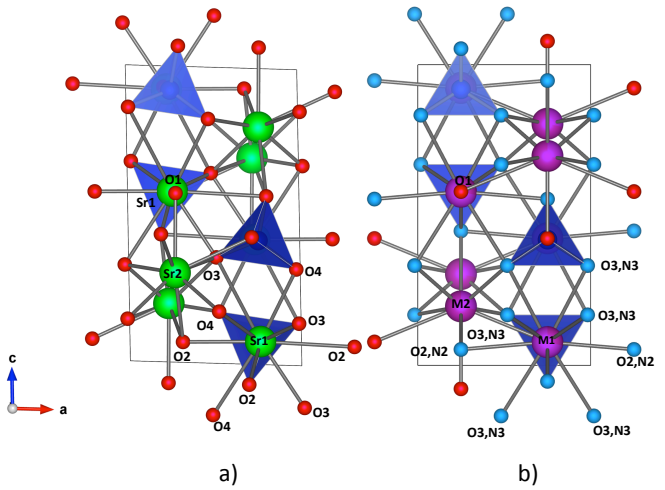


a) b)

**Fig. 1.** Crystal structures of a) the β polymorph of $Sr_2SiO_4$ and b) the oxynitridosilicates $LaMSiO_3N$ (M= Sr, Ba, Eu) isostructural to the α' polymorph of $Sr_2SiO_4$ and $Ba_2SiO_4$. In $LaMSiO_3N$ M1 sites show occupancies of c.a. 75 % for M=Sr, Eu and 80 % for M=Ba whereas M2 sites show the same occupancies for $La^{3+}$ cations. [27]

temperature by doping with a larger cation as $Ba^{2+}$ or with $Eu^{2+}$ and is the only one reported for $Ba_2SiO_4$. We have recently shown that the compounds $LaMSiO_3N$ (M= Sr and Ba) crystallize in the Pmnb structure (Figure 1b) [27] and are isostructural to $LaEuSiO_3N$.[28] They represent one of the few reported examples of oxynitride orthosilicates, and contain isolated $[SiO_3N]^{5-}$ tetrahedra. These oxynitrides show partial order of La and the alkaline earth cations in the two sites M1 and M2, with preferred occupancy of $La^{3+}$ (c.a. 75 % for $LaSrSiO_3N$ and 80 % for $LaBaSiO_3N$) at the nine-coordinated M2 sites as well as partial nitrogen order in sites X2 and X3 of the $\beta$-$K_2SO_4$ structure. The activation of $LaSrSiO_3N$ or $LaBaSiO_3N$ with $Eu^{2+}$ or $Ce^{3+}$ leads to luminescent materials with emission wavelenghts up to 700 nm under excitation with UV-blue light.[27] In this paper we report the synthesis, structural characterization by synchrotron radiation X-ray powder diffraction and luminescent properties of several members of the new solid solution $Sr_{2-x}La_xSiO_{4-x}N_x$ ($0 \le x \le 1$) activated with $Eu^{2+}$ or $Ce^{3+}$ that show a wide range of emission wavelengths tuned as a function of the La/N content.

## 2. Experimental

### 2.1 Synthesis

Samples with compositions $Sr_{2-x}La_xSiO_{4-x}N_x$ (x=0, 0.2, 0.3, 0.5, 0.8, 1), $Sr_{1.98-x}Eu_{0.02}La_xSiO_{4-x}N_x$ (x=0, 0.2, 0.3, 0.5, 1) and $Sr_{2-x}La_{x-0.02}Ce_{0.02}SiO_{4-x}N_x$ (x=0.2, 0.3, 1) were prepared by solid state reaction in $N_2/H_2$ (95 % / 5 % V/V, Air Liquide, 99.999 %) of stoichiometric mixtures of $La_2O_3$ (Aldrich, 99.99 %), SrO, $Si_3N_4$ (α-phase, Alfa Aesar, 99.9 %), $SiO_2$ (Aldrich, 99.995 %) and $Eu_2O_3$ (Aldrich, 99.99 %) or $CeO_2$ (Aldrich, 99.995 %). $La_2O_3$, $Eu_2O_3$, $SiO_2$ and $CeO_2$ were previously treated in air at 950 °C for 4 h. SrO was prepared by overnight decomposition of $SrCO_3$ (Alfa Aesar, 99.994 %) at 1000 °C under a dynamic vacuum of 5 Pa. Handling of SrO was carried out in a Glovebox under recirculating argon atmosphere. The powders were thoroughly mixed in an agate mortar for 30 min, pressed into pellet, placed in a molybdenum crucible and covered with zirconium foil that acts as an oxygen/water scavenger. The mixtures were fired at 1500 °C during 3 hours with heating and cooling rates of 300 °C/h. EDS analyses were performed in a FEI Quanta 200 FEG scanning electron microscope equipped with a EDAX detector with an energy resolution of 132 eV. Nitrogen contents were determined by combustion analysis and TGA in pure oxygen. Combustion analysis was performed in a Thermo Fisher Scientific instrument heating the sample up to 1060 °C, using MgO, $WO_3$ and Sn as additives and atropine as a reference standard. Thermogravimetric analysis in pure oxygen was performed in a NETZSCH-STA 449 F Jupiter. The samples were heated at 10 °C/min to 1200 °C under $O_2$ at a flow rate of 70 $cm^3$/min.

### 2.2 Structural Characterization

X-ray powder diffraction data were collected on a Rigaku diffractometer (for samples with x=1) and on a Siemens D5000 diffractometer using Cu Kα radiation (λ= 1.5418 Å). Synchrotron X-ray powder diffraction data were collected at room temperature on the 11-BM instrument at the Advanced Photon Source (APS), Argonne National Laboratory using λ= 0.458996 Å. Rietveld analysis was carried out using the program Fullprof.[29] Background refinement was performed either by linear interpolation or by using a polynomial function. Temperature factors were refined anisotropically for heavy atoms and for some anion positions. Electron diffraction micrographs were obtained in a JEOL 1210 transmission electron microscope operating at 120 kV, equipped with a side-entry 60°/30° double tilt GATAN 646 specimen holder. The samples were prepared by dispersing the powders in hexane and depositing a droplet of this suspension on holey carbon film supported on a copper grid.

### 2.3 Optical Characterization

Micro-photoluminescence (μ-PL) emission spectra were measured at room temperature using the 405 nm line of a solid-state laser for excitation on a LabRam HR800 high resolution spectrometer equipped with a charge-coupled device detector. The spectra were corrected for the response of the spectrometer by normalizing each spectrum employing the detector and grating characteristics. The incident light power density was about 1 W/$cm^2$. The excitation spectra were measured on a Horiba Jobin Yvon FluoroMax-4 spectrofluorometer equipped with a xenon lamp, a photomultiplier detector (range 200 nm to 850 nm) and a photodiode reference detector. Photoluminescence quantum yield (PLQY) was measured using a Horiba Quanta-ϕ, 6 in.

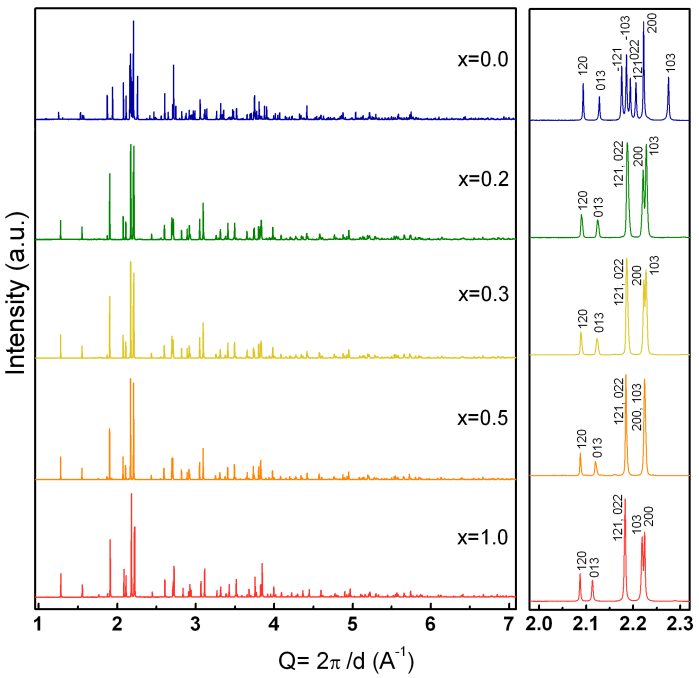


**Fig. 2.** High resolution synchrotron X-ray diffraction patterns of $Sr_{2-x}La_xSiO_{4-x}N_x$ samples ($0 \le x \le 1$) and enlarged images of the intense reflections around Q=2 $Å^{-1}$ region.

diameter, spectralon-coated integrating sphere. The phosphor powders were encapsulated in silicone resin (GE Silicones, RTV-615) and deposited on transparent quartz substrates (Chemglass). A neutral density filter and a long pass filter (LPF430) were used to prevent saturation of the detector on the excitation acquisition and to cut off the second harmonic at the emission measurement, respectively. A Correction factor was introduced in the PLQY calculus to take into account the wavelength dependent attenuation introduced by the integrating sphere and the filters. Diffuse reflectance spectra were registered at room temperature on a UV-Vis-NIR Varian Cary 5000 spectrophotometer, with operational range of 190-3300 nm.

## 3. Results and discussion

### 3.1 Synthesis and crystal chemistry of the solid solution $Sr_{2-x}La_xSiO_{4-x}N_x$ ($0 \le x \le 1$)

Figure 2 shows high resolution synchrotron X-ray diffraction patterns of selected samples of the solid solution $Sr_{2-x}La_xSiO_{4-x}N_x$ ($0 \le x \le 1$). Reconstruction of the reciprocal lattice from electron diffraction patterns confirmed the $P2_1/n$ symmetry for $Sr_2SiO_4$ and Pmnb space group for samples with $x \neq 0$. The transition from the β polymorph to the α' phase is observed for $x \geq 0.2$. X-ray diffraction patterns of the $Eu^{2+}$ or $Ce^{3+}$ doped samples were similar to those of the corresponding undoped compounds showing the same monoclinic (for x=0) or orthorhombic symmetry (for $x \geq 0.2$) (See ESI, Fig. S1 and S2).

The observed and calculated synchrotron X-ray diffraction patterns obtained by Rietveld refinement for the undoped compounds are shown in figure 3 for the sample with x=0.5 and in supporting information for all samples (See ESI, Fig. S3).

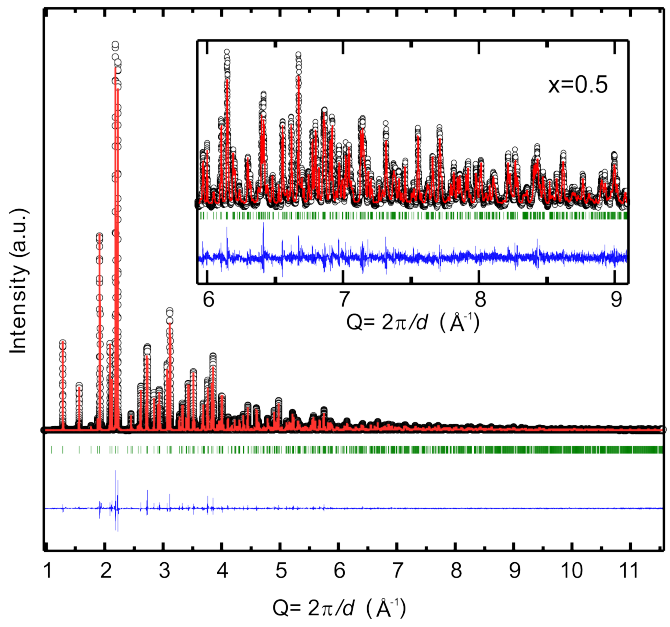


**Fig. 3.** Observed and calculated synchrotron X-ray powder diffraction patterns for $Sr_{1.5}La_{0.5}SiO_{3.5}N_{0.5}$.

The refinements indicated that the samples did not contain any significant impurity. The summary of crystallographic and refinement data are shown in Table S1, and Table S2 (ESI) shows the atomic coordinates and refined La/Sr occupancies for the sample with x=0.5. Refinement of La occupancies for samples with x=0.2, 0.3 lead to negative values for site M1, and the % of the total La content in the two cation sites were fixed to those refined in the sample with x=0.5. For x=0.5 the refined occupancies obtained by fixing the ratio of La:Sr to the nominal stoichiometries were 0.054(9) and 0.446 for La at sites 1 and 2 respectively. In agreement with previous results obtained for $LaSrSiO_3N$ and $LaBaSiO_3N$, [27] this cation distribution shows a preferential occupation of $La^{3+}$ with smaller ionic radius than $Sr^{2+}$ of the nine coordinated site. [30] Anion occupancies for sites X1, X2 and X3 were fixed according to those found for $LaBaSiO_3N$ in our previous neutron diffraction experiment where O/N ratios of 1/0, 0.55/0.45 and 0.73/0.27 were obtained for the three sites respectively (See Fig. 1b). Considering the coordination of M1 (3 X2, 6 X3, 1 X1) and M2 (2 X2, 4 X3, 3 X1) the anion distributions found in the two polyhedra of the barium compound were [M1 $O_{6.7}$ $N_{3.3}$] and [M2 $O_{6.8}$ $N_{2.2}$] which corresponds to an average N/O ratio larger for M1 than for M2 (N/O= 0.49 and 0.32 respectively).[27] Quantitative EDS analyses of individual particles of each sample confirmed the cationic La:Sr:Si ratios and indicated that the samples were compositionally homogeneous. The average La:Sr:Si ratios obtained from c.a. 10 individual particles for each sample were 0.2:1.8:1.1 (x=0.2), 0.3:1.7:1.0(x=0.3), 0.6:1.5:1.0(x=0.5) and 0.9:1.0:0.1.2(x=1) which agree well with the nominal compositions within the standard deviations.

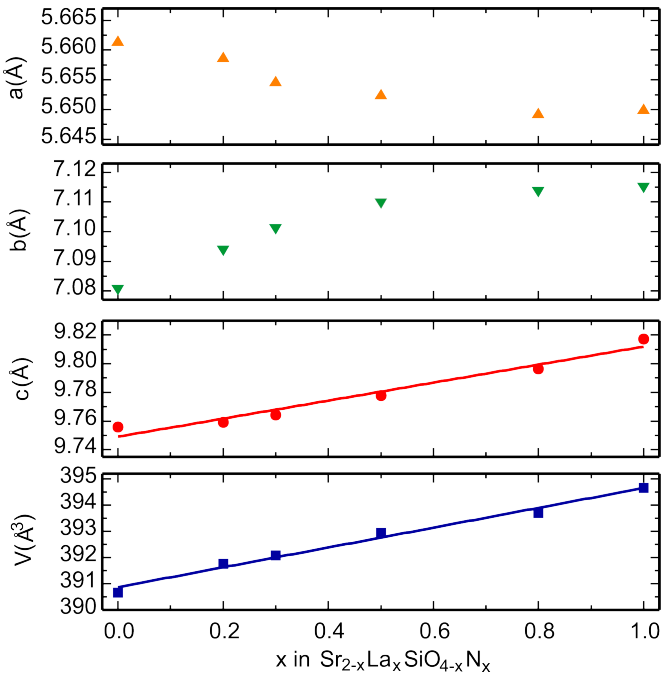


**Fig. 4.** Refined parameters from synchrotron X-ray powder diffraction data of $Sr_{2-x}La_xSiO_{4-x}N_x$ samples as a function of La/N content. The parameters of sample with x=0.8 were obtained from laboratory X-ray diffraction data.

Nitrogen contents determined by chemical analyses were respectively 0.20(2), 0.28(2), 0.50(2) and 1.00(2) per formula. These results showed that the substitutions in $Sr_2SiO_4$ of Sr by La and of O by N occur as a charge compensation mechanism. Nitrogen contents determined by TGA in oxygen were consistent with results of chemical analyses. The decomposition of the samples to the oxides started at temperatures between 550 °C (for x=1) and 750 °C (for x=0.2). For the samples with larger nitrogen contents the weight increased to a maximum and then decreased at higher temperatures. (See Figure S4 (ESI)) This behaviour is typical of oxynitrides and it has been interpreted through the formation of intermediate phases with weakly bonded $N_2$ molecules.[31] The observed *vs* calculated weight increases at 1000 °C were for x=0.2: 1.1 %/0.7 %; x=0.3: 1.4 %/1.1 %; x=0.5: 1.9 %/ 1.7 %; x=1: 3.0 %/3.2 %.

Figure 4 shows the variation of the refined cell parameters and unit cell volumes with La/N contents and figure 5 shows the variation on x of the bond valence sums (BVS) and other structural parameters for sites M1 and M2. The effect of the substitution of Sr and O by La and N respectively is stronger on the b and c axes. Both parameters as well as the cell volume increase with x showing that the increase of $N^{3-}$ with larger ionic radius than $O^{2-}$ (r $O^{2-}$ = 1.38 Å (CN IV); r$N^{3-}$ = 1.46 Å (CN IV))[30] outweighs the introduction of $La^{3+}$ which is smaller than $Sr^{2+}$. The stabilization of the α' phase at room temperature observed for x≥0.2 is most likely a consequence of the increase in bond valence of M1 site produced by the introduction of the more charged anion $N^{3-}$. The bond valence sums [32, 33] for Sr at this site are 1.78 for β-$Sr_2SiO_4$[27, this work] and 1.58 for α'-$Sr_2SiO_4$ whereas in the solid solution $Sr_{2-x}La_xSiO_{4-x}N_x$ it increases

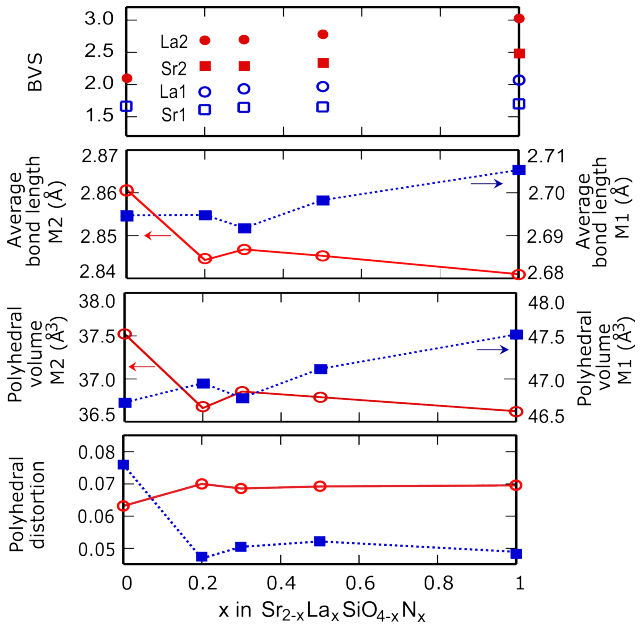


**Fig. 5**. Bond valence sums, average bond distances and polyhedral volumes and distortions of sites M1 (blue points, dotted line) and M2 (red points, solid line) in $Sr_{2-x}La_xSiO_{4-x}N_x$.

up to 1.69 (for $LaSrSiO_3N$). The major changes observed between x=0 and x=0.2 in bond lengths of M2 site, polyhedral distortion and polyhedral volume are a consequence of the change in symmetry from monoclinic (β' phase) to orthorhombic (α' phase). The average bond length and the polyhedral volume in site M1 increase with x as a consequence of the effect of nitriding that overcompensates the contraction induced by the substitution of $Sr^{2+}$ by the smaller $La^{3+}$. In M2 site the reduction in the polyhedral volume with increasing x is caused by the large proportion of $La^{3+}$ (75 % for x=1) which is more important than the expansion caused by the introduction of $N^{3-}$.

### 3.2 Photoluminescent properties

The excitation and emission spectra of $Sr_{2-x}La_xSiO_{4-x}N_x$:0.02 $Eu^{2+}$ samples (x=0, 0.2, 0.3, 0.5 and 1) are shown in Figure 6 and Figure 7 shows the diffuse reflection spectra for samples with x≥0.2. The excitation spectra collected at 550 nm consist of a broad band centered between 350 nm (for x=1) and 375 nm (for x=0). With increasing N/La content the excitation band narrows and shifts gradually towards shorter wavelengths. The diffuse reflection spectra of doped samples show the absorption of the host and a wide band in the region from 300 to 500 nm corresponding to the $4f^7 \rightarrow 4f^6 5d^1$ transition of $Eu^{2+}$. In agreement with the excitation spectra the absorption edge of the host is shifted towards lower energies with increasing x which leads to a progressive increase of the overlap between this band and the $4f^7 \rightarrow 4f^6 5d^1$ band. The observed emission upon excitation at 405 nm consists of a broad band centered between 550 nm (for x=0) and 650 nm (for x=1) with maximum intensity at c.a. 700 nm for x=1. This band can be assigned to the parity allowed $4f^6 5d^1 \rightarrow 4f^7$ transition of $Eu^{2+}$ and it can be

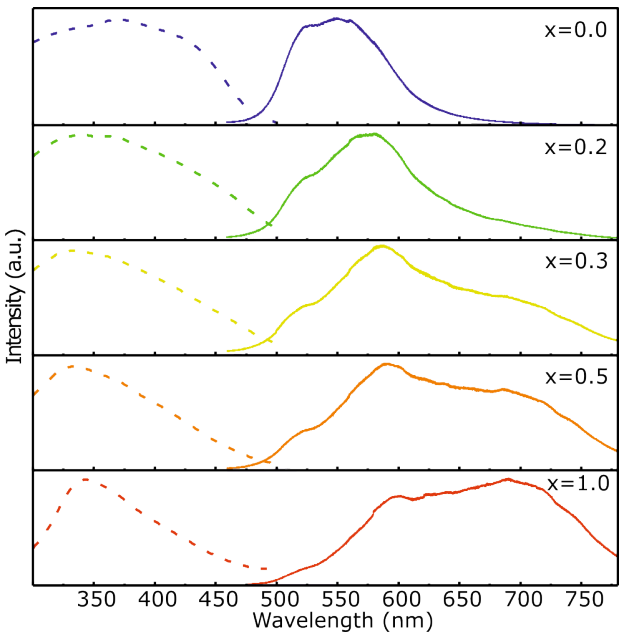

**Fig. 6.** Normalized excitation ($\lambda_{emiss}$= 550 nm, dotted line) and emission spectra ($\lambda_{exc}$= 405nm, solid line) collected at room temperature for $La_xSr_{2-x}SiO_{4-x}N_x$ : 0.02 $Eu^{2+}$ samples.

deconvoluted into two main components corresponding to M1 and M2 sites as in previously reported $Ba_2SiO_4:Eu^{2+}$, $Sr_2SiO_4:Eu^{2+}$ and $LaMSiO_3N$:Eu (M=Sr, Ba). [16, 17, 27] The best fits of the spectra of samples with x≥0.3 are obtained with two additional components which can be ascribed to different environments around $Eu^{2+}$ resulting from the mixed occupation of $Sr^{2+}$ and $La^{3+}$ in the two crystallographic sites. The concomitant substitution of one Sr by La and one O by N in $Sr_2SiO_4$ produces, in addition to the red shift of the centroid of the band of c.a. 100 nm, an important broadening, from fwhm=100 nm for x=0 to fwhm=200 nm for x=1. For x=0 the band at higher energy is assigned to the M2 site and has lower intensity than the M1 band. The respective wavelengths of these bands are 518 and 560 nm (See ESI, Fig. S5). For x>0 a new component with λ between 679 and 706 nm is observed, with increasing intensity as La content increases. In our previous study of $LaMSiO_3N$: Eu (M= Sr, Ba) we tentatively assigned this band to M1 site, red shifted by the introduction of nitride. However the dependence of the intensity of this band with La content suggests that it is most likely due to the M2 sites occupied by the small and charged $La^{3+}$ (75 % of M2 sites in $LaSrSiO_3N$) that generates a stronger crystal field splitting than $Sr^{2+}$. The additional effects of covalency and large crystal field splitting caused by the introduction of nitride would induce the observed important red shift of c.a. 190 nm in this band with respect to $Sr_2SiO_4:Eu^{2+}$. The increase in intensity of this band is concomitant with the decrease in intensity of the band with highest energy centered between 518 nm (for x=0) and 528 nm (for x=1) which is assigned to the c.a. 25 % of M2 sites occupied by $Sr^{2+}$. According to this the central band at 560-590 nm would be assigned to the M1

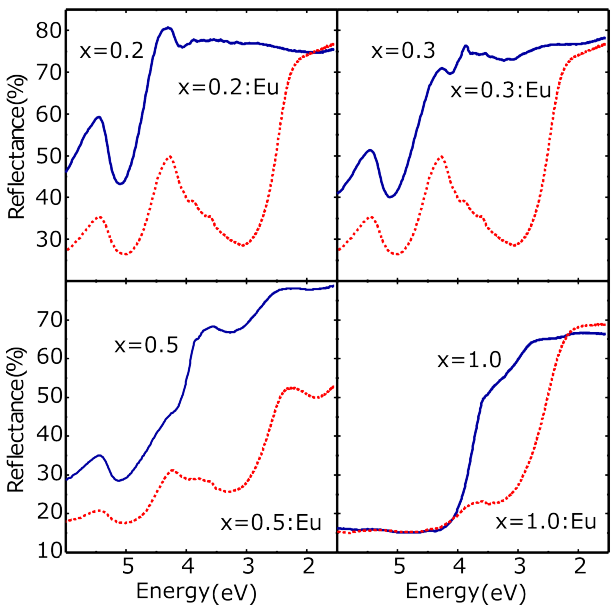


**Fig. 7.** Diffuse reflectance spectra collected at room temperature for $Sr_{2-x}La_xSiO_{4-x}N_x$ (blue solid line) and $Sr_{2-x}La_xSiO_{4-x}N_x$: 0.02 $Eu^{2+}$ (red dotted line) samples.

sites occupied by $Sr^{2+}$ (80 % of M1 sites in $LaSrSiO_3N$), and a weak small component at c.a. 640 nm would be due to the M1 sites occupied by $La^{3+}$(20 % of M1 sites in $LaSrSiO_3N$). The energies of all components shift to the red with increasing N/La substitution, as a result of the increase in covalency and the crystal field splitting. The large band broadening is most likely caused by the different N/O proportion in the M1 and M2 sites and crystal field splitting's that would lead to different red-shift of the corresponding $Eu^{2+}$ emissions. As a result of the red shift of the emission band and the blue shift of the excitation band the Stokes shift increases 175 nm from x=0 to x=1. All samples can be excited at near UV light (405 nm) and samples with x≤0.3 can also be excited with blue (450 nm) light. As for the $Eu^{2+}$ activated compounds the deconvolution of emission spectra of $Sr_{2-x}La_xSiO_{4-x}N_x$:0.02 $Ce^{3+}$ samples (x= 0.2, 0.3, 1) (Figure 8 and ESI) show two main components ascribed to the crystallographic sites M1 and M2 and two additional bands resulting from the mixed occupation of these sites by $La^{3+}$ and $Sr^{2+}$ . The range of wavelengths observed for the four components in this case are 680-690 nm, 620-633 nm, 558-577 nm and 511-515 nm with red shifting as $La^{3+}$ content increases. Orange-red luminescence in (oxy)nitride $Ce^{3+}$ activated compounds has been reported for $CaSiN_2$, [6] $La_3Si_6N_{11}$, [34] or $La_{10}Ge_6N_{2.46}O_{23.31}$ . [35] In $Sr_{2-x}La_xSiO_{4-x}N_x$:0.02 $Ce^{3+}$ the observed long emission wavelenghts are a consequence of the strong effect of the covalence of Ce-N bonds and crystal field splitting induced by $N^{3-}$ enhanced by the introduction of $La^{3+}$. The transition energies observed for both activators in a given member of the solid solution are related in agreement with the empirical correlation reported by Dorenbos for $Eu^{2+}$ and $Ce^{3+}$ in inorganic compounds. [36]

The CIE (Commission Internationale del'Eclairage) 1931 chromaticity diagram of $Sr_{2-x}La_xSiO_{4-x}N_x:Eu^{2+}$ (x=0, 0.2, 0.3, 0.5

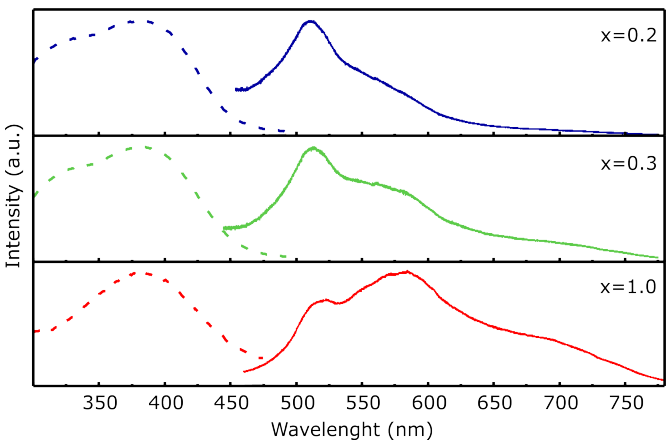


**Fig. 8.** Normalized excitation ($\lambda_{emiss}$= 550 nm, dotted line) and emission spectra ($\lambda_{exc}$= 405 nm, solid line) collected at room temperature for $Sr_{2-x}La_xSiO_{4-x}N_x$: 0.02 $Ce^{3+}$ samples.

and 1) and $Sr_{2-x}La_xSiO_{4-x}N_x:Ce^{3+}$ (x= 0.2, 0.3 and 1) phosphors (Figure 9) illustrates the wide range of colors that can be obtained by changing the La and N content in this host. The emission color shifts in $Sr_{2-x}La_xSiO_{4-x}N_x:Eu^{2+}$ from green-yellow for x=0 (chromaticity coordinates x=0.366, y=0.572) to orange-red (chromaticity coordinates x=0.528, y=0.4232) for x=1. The largest change in the chromaticity coordinates is appreciated for the sample with x=0.2. For $Sr_{2-x}La_xSiO_{4-x}N_x:Ce^{3+}$ the emission color changes from blue-green for x= 0.2 (chromaticity coordinates x=0.260, y=0.398) to orange-yellow for x=1 (x=0.432, y=0.449). As the CIE colour rendering index is based on human eye physiological perception of color all spectral emission above 700 nm do not contribute to the chromaticity coordinates. Consequently the large increase in intensity of the red emission of $Eu^{2+}$ phosphors with x≥0.2 leads to a slight contribution to the shift into the red region of the CIE diagram.

The photoluminescent quantum yield (PLQY) of $Sr_{2-x}La_xSiO_{4-x}N_x:Eu^{2+}$ phosphors was calculated using the method by Palsson et al.[37] that uses the equation:

$$\phi_f = \frac{(E_C - E_A)}{(L_A - L_C)}$$

where $E_C$ is the integrated luminescent of the sample, $E_A$ is integrating luminescence of the empty integrating sphere, $L_A$ is the integrated excitation profile of the empty integrating sphere and $L_C$ is the integrated excitation profile of the sample.[38] A decrease of PLQY is observed as La/N content increases through the solid solution, with 72 % shown for x=0, 33 % for x=0.2, 26 % for x=0.3, 20 % for x=0.5 and 4 % for x=1. In the $Ce^{3+}$ samples the observed quantum yields are 16 % for x=0.2, 12 % for x=0.3 and 1 % for x=1. The large Stokes shift observed in these phosphors indicates a strong coupling of the 5d electrons with phonons. Thermal quenching seems to be the most plausible mechanism for the non-radiative relaxation of

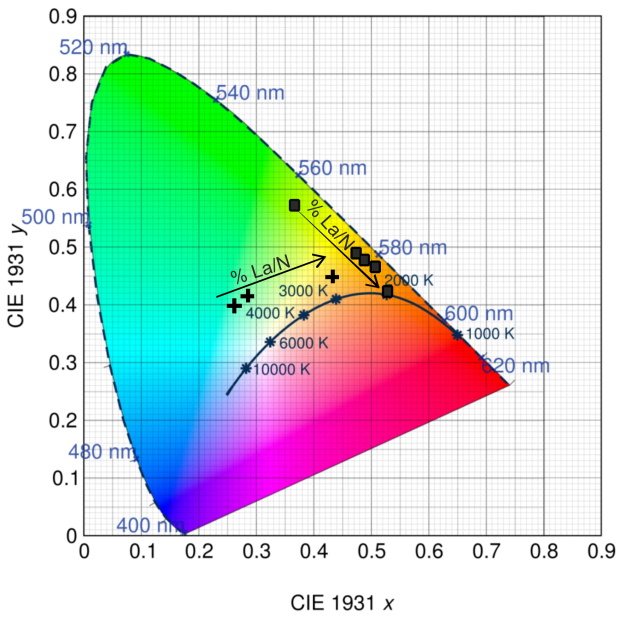


**Fig. 9**. CIE diagram showing the change of emission colour in $Sr_{2-x}La_xSiO_{4-x}N_x$ activated with $Eu^{2+}$ (from green to red, square markers) and with $Ce^{3+}$ (from blue to yellow, cross markers).

the excited state of the rare earth. The substitution of $Sr^{2+}$ by $La^{3+}$ contributes to lower the conduction band of the host reducing the energy difference between the lowest 5d state of the activator and the bottom of the conduction band, increasing the probability of a thermal promotion of the 5d electrons to the conduction band. This photoionization process has been described as one of the primary mechanisms for non radiative transitions and consequent decrease of quantum efficiency.[39]

## Conclusions

The compounds $Sr_2SiO_4$ and $LaSrSiO_3N$ are end members of the solid solution $Sr_{2-x}La_xSiO_{4-x}N_x$ (0≥x≥1) that is formed by charge balanced substitution of $Sr^{2+}$ by $La^{3+}$ and $O^{2-}$ by $N^{3-}$ in the strontium orthosilicate. The introduction of lanthanum and nitrogen induces a phase transition from the β phase to α' isostructural to β-$K_2SO_4$ for x=0.2, stabilizing this polymorph at room temperature. As for $LaSrSiO_3N$, in intermediate members of the solid solution the $La^{3+}$ cations occupy preferentially the 9th coordinated position of the β-$K_2SO_4$ structure. The β→α' transition is most likely induced by the increase in bond valence of the underbonded cations at M1 sites which is caused by nitriding. The introduction of $La^{3+}$ allows the doping with $Ce^{3+}$ cations in the $Sr_2SiO_4$ structure in addition to $Eu^{2+}$. Photoluminescence measurements of doped compounds with 0.02 $Eu^{2+}$ or 0.02 $Ce^{3+}$ per formula revealed that the La/N introduction in $Sr_2SiO_4$ produces an important red-shift of the emission, peaking at 580-700 nm for $Eu^{2+}$ samples and at 580 nm for $Ce^{3+}$ samples under excitation at 405 nm. The emission colour is tuned by the La/N stoichiometry from green-yellow (x=0) to orange-red (x=1) for $Eu^{2+}$ phosphors and from blue-green (x=0.2) to orange-yellow (x=1) in $Ce^{3+}$ samples providing a new family of luminescent orthosilicate oxynitride materials with β-$K_2SO_4$ structure with a wide range of emission wavelengths. Further increase of emission colours range in this family of materials would be expected by substitution of $La^{3+}$ by $Y^{3+}$ or $Sr^{2+}$ by $Ca^{2+}$, and by increasing lanthanum/ nitrogen contents in the host oxynitrides.

## Acknowledgements

This work was supported by the Spanish Ministerio de Economia y Competitividad, Spain (Project MAT2014-53500-R), and it has been developed under the Materials Science PhD program of the Universitat Autònoma de Barcelona. Fellowship support to AB from Ministerio de Economía, Spain (FPI, project MAT2011-24757) and to KAD from the ConvEne IGERT Program (NSF-DGE 0801627), are gratefully acknowledged. AB thanks the ICMR at UCSB for hospitality, supported by the IMI Program of the National Science Foundation under Award No. DMR 08-43934. This study made

use of MRL Central Facilities, which was supported by the MRSEC Program of the NSF under Award No. DMR 1121053. Use of the Advanced Photon Source at Argonne National Laboratory was supported by the U.S. Department of Energy, Office of Science, Office of Basic Energy Sciences, under Contract no. DE-AC02-06CH11357. Dr. Judith Oró-Solé is acknowledged for TEM studies and for performing EDS analyses.

## Notes and references


1 I. Azevedo, M. G. Morgan and F. Morgan, Proceedings of the IEEE, 2009, **97**, 481-510.
2 G. F. Shuji Nakamura, *The Blue Laser Diode*, Springer-Verlag Berlin Heidelberg 1997.
3 V. Bachmann, C. Ronda, O. Oeckler, W. Schnick and A. Meijerink, *Chem. Mat.*, 2009, **21**, 316.
4 J. E. J. van Steen, J. W. H. van Krevel, G. Botty, A. C. A. Delsing, Y. Q. Li, G. de With, H. T. Hintzen, F. J. DiSalvo, G. de With and H. T. Hintzen, *J. All. Comp.*, 2006, **417**, 273.
5 Y. Sato, H. Kato, M. Kobayashi, T. Masaki, D.-H. Yoon and M.Kakihana, *Angew. Chem. Int. Ed.*, 2014, **53**, 7756.
6 R. Le Toquin and A. K. Cheetham, *Chem. Phys. Lett.*, 2006, **423**, 352.
7 K. Uheda, N. Hirosaki, Y. Yamamoto, A. Naito, T. Nakajima and H. Yamamoto, *Electr. Sol. State Lett.,* 2006, **9**, H22.
8 J.Zhou, Z.Xia, M.Chen, M.S.Molokeev and Q.Liu, *Sci. Rep.*, 2015, **5**, 12149.
9 A. Fuertes, *Dalton Trans.,* 2010, **39**, 5942.
10 H.A. Höppe, H. Lutz, P. Morys, W. Schnick and A.J. Seilmeier, *Phys. Chem. Sol.,* 2000, **61**, 2001.
11 M. Zeuner, S. Pagano and W. Schnick, *Angew. Chem. Int. Ed.*, 2011, **50**, 7754.
12 R-J Xie and T.B. Hintzen, *J. Amer. Cer. Soc*., 2013, **96**, 665.
13 N. George, K. Denault and R. Seshadri, *Ann. Rev. Mat. Sci.*, 2013, **43**, 481.
14 P. Pust, V. Weiler, C. Hecht, A. Tücks, A.S. Wochnick, A-K. Henb, D. Wiechert, C. Scheu, P.J. Schdmidt, and W. Schnick, *Nat. Mat.,* 2014, **13**, 891.
15 A.Fuertes, *Mater. Hor.* 2015, **2**, 453.
16 S.H.M. Poort, W. Janssen and G. Blasse, *J. All. Comp.* 1997, **260**, 93.
17 J. Kim, Y. Park, S. Kim, J. Choi and H. Park, *Sol. State Comm.*, 2005, **133**, 445.
18 J. K. Han, M. E. Hannah, A. Piquette, G. A. Hirata, J. B. Talbot, K. C. Mishra and J. McKittrick, *J. Luminesc.* , 2012, **132**, 106.
19 K. Denault, J. Brgoch, M. Gaultois, A. Mikhailovsky, R. Petry, H. Winkler, S. DenBaars and R. Seshadri, *Chem. Mat.*, 2014, **26**, 2275.
20 T.L. Barry, *J. Elect. Soc.* 1968, **115**, 1181.
21 P. Dorenbos, *J. Luminescence*, 2003, **104**, 239.
22 J.K. Park, M.A.Lim, C.H.Kim, H.D.Park, J.T.Park and S.Y.Choi, *Appl. Phys. Lett.*, 2003, **82**, 683.
23 S.Miao, Z.Xia, M.S.Molokeev, M.Chen, J.Zhang and Q.Liu, *J. Mater. Chem. C*, 2015, **3**, 4616.
24 M. Catti, G. Gazzoni and G. Ivaldi, *Acta Cryst.. Sect. C, Crystal Str. Comm.*, 1983, **39**, 29.
25 M.Catti, G.Gazzoni, G.Ivaldi and G.Zanini, *Acta Cryst.,* 1983, **B39**, 674.
26 L. Stenberg, J.R. Sellar and B.G. Hyde, *Nature*, 1986, **320**, 428.
27 A. P. Black, K. A. Denault, J. Oro-Sole, A. R. Goni and A. Fuertes, *Chem. Comm.*, 2015, **51**, 2166.
28 R. Marchand, *C.R. Acad. Sci. Paris*, 1976, **283**, 281.
29 J.Rodríguez-Carvajal, *Phys. B*, 1993, **192**, 55.
30 R. D. Shannon, *Acta Crystallogr., Sect. A: Cryst. Phys. Diffr. Theor. Gen. Crystallogr.*, 1976, **32**, 751.
31 F. Tessier, L. Le Gendre, F. Chevire, R. Marchand and A. Navrotsky, Chem. Mater., 2005, **17**, 3570.
32 I.D. Brown and D. Altermatt, Acta Cryst. 1985, **B41**, 244.
33 N.E. Brese and M. O'Keeffe, *Acta Cryst.* **B47**, 1991, 192.
34 T.Suerhiro, N.Hirosaki and R.-J-Xie, *ACS Appl. Mater. Interfaces*, **3**, 2011, 811.
35 S. Thomas, J. Oró-Solé, B. Glorieux, V. Jubera, V. Buissette, T. Le Mercier, A. Garcia and A. Fuertes, *J. Mater. Chem.,* 2012, **22**, 23913.
36 P.Dorenbos, *J. Phys.:Condens. Matter*, 2003, **15**, 4797.
37 L. O. Palsson and A. P. Monkman, *Adv. Mat.,* 2002, **14**, 757.
38 J. Hou, X. Yin, Y. Fang, F. Huang and W. Jiang, *Opt. Mat.*, 2012, **34**, 1394.
39 P. Dorenbos, *J. Phys. Cond. Matt.*, 2005, **17**, 8103.

# Emission colour tuning through coupled N/La introduction in $Sr_2SiO_4$: $Eu^{2+}$

Ashley P. Black, Kristin A. Denault, , Carlos Frontera, Ram Seshadri , Alejandro R. Goñi, and Amparo Fuertes

# Supplementary Information

**Table S1.** Crystallographic and refinement data from synchrotron X-ray powder diffraction data (λ=0.458996 Å, T=298 K) for $Sr_{2-x}La_xSiO_{4-x}N_x$ (x= 0.0, 0.2, 0.3, 0.5, 1.0) .

| | **β-$Sr_2SiO_4$** | **$La_{0.2}Sr_{1.8}SiO_{3.8}N_{0.2}$** | **$La_{0.3}Sr_{1.7}SiO_{3.7}N_{0.3}$** | **$La_{0.5}Sr_{1.5}SiO_{3.5}N_{0.5}$** | **$LaSrSiO_3N$** |
|---|---|---|---|---|---|
| Space group | $P2_1/n$ | Pmnb | Pmnb | Pmnb | Pmnb |
| a(Å) | 5.6613(1) | 5.65855(1) | 5.6545(1) | 5.6523(1) | 5.64986(5) |
| b(Å) | 7.0808(1) | 7.0942(1) | 7.1014(1) | 7.1100(1) | 7.11547(5) |
| c(Å) | 9.7558(1) | 9.7591(2) | 9.7641(2) | 9.7778(2) | 9.8172(1) |
| β(°) | 92.6515(8) | | | | |
| V(Å$^3$) | 390.66(1) | 391.76(1) | 392.08(1) | 392.95(1) | 394.67(1) |
| $N_p$, $N_{irefl}$ [(a)] | 34500, 2617 | 34500, 1394 | 34500, 1403 | 34500, 1400 | 34500, 1435 |
| $P_p$, $P_i$, $P_g$ [(b)] | 17, 63, 7 | 13, 24, 39 | 15, 24, 6 | 15, 29, 7 | 13, 26, 7 |
| $R_{Bragg}$, $R_f$, $\chi^2$ | 5.0, 3.0, 1.43 | 4.16, 5.06, 1.38 | 4.88, 4.81, 2.01 | 4.15, 3.6, 2.70 | 3.43, 3.88, 1.37 |
| $R_p$, $R_{wp}$, $R_{ex}$ [(c)] | 9.20, 13.6, 11.34 | 9.51, 13.0, 11.13 | 8.98, 13.3, 9.45 | 9.79, 14.4, 8.73 | 5.98, 9.38, 8.02 |

(a) $N_p$, $N_{irefl}$ refer to the number of experimental points and independent reflections.

(b) $P_p$, $P_i$, $P_g$, refer to the number of profile, intensity-affecting and global refined parameters, respectively.

(c) Conventional Rietveld R-factors ($R_p$, $R_{wp}$ , $R_{exp}$) in %

**Table S2**. Atomic coordinates, cation and anion occupancies for $Sr_{1.5}La_{0.5}SiO_{3.5}N_{0.5}$ [(a,b)]

| **Site** | **Wyckoff position** | **x** | **y** | **z** | **occupation factor** |
|---|---|---|---|---|---|
| La1/Sr1 | 4c | 0.25 | 0.6575(7) | 0.4175(3) | 0.054(9)/0.946 |
| La2/Sr2 | 4c | 0.25 | 0.0055(7) | 0.42182(6) | 0.446/0.554 |
| Si | 4c | 0.25 | 0.221(2) | 0.6966(5) | 1 |
| O1/N1 | 4c | 0.25 | 0.9950(5) | 0.4343(4) | 1/0 |
| O2/N2 | 4c | 0.25 | 0.331(8) | 0.570(5) | 0.5/0.5 |
| O3/N3 | 8d | 0.012(5) | 0.286(4) | 0.338(4) | 0.75/0.25 |

(a) Estimated standard deviations in parentheses are shown once for each independent variable. La/Sr occupation factors were refined subject to the ideal stoichiometry. O/N occupation factors were considered fixed to those obtained in $LaBaSiO_3N$ from neutron diffraction in A. P. Black, K. A. Denault, J. Oro-Sole, A. R. Goñi and A. Fuertes, Chem. Comm., 2015, 51, 2166.

(b) Refined isotropic B-factors were 0.83(3) Å$^2$ for silicon, 2.06(9) Å$^2$ for O2/N2 and 1.74(7) Å$^2$ for O3/N3. Temperature factors were refined anisotropically for La/Sr and O1/N1. Resulting equivalent B-factors were 1.29 Å$^2$, 0.99 Å$^2$ and 2.95 Å$^2$ for La1/Sr1, La2/Sr2 and O1/N1, respectively.

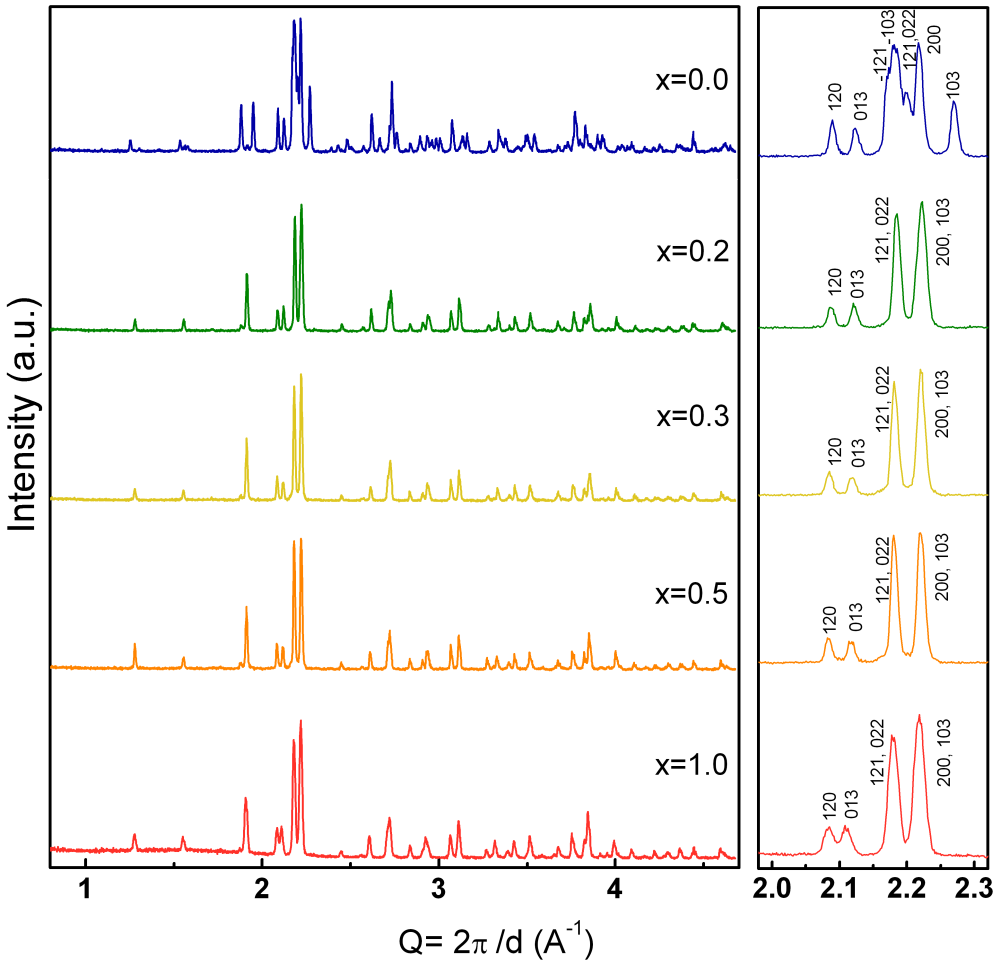


**Figure S1. X-ray powder diffraction patterns for $Sr_{1.98-x}Eu_{0.02}La_xSiO_{4-x}N_x$ ($0 \geq x \geq 1$) and enlarged images of the intense reflections around Q=2 Å $^{-1}$ region.**

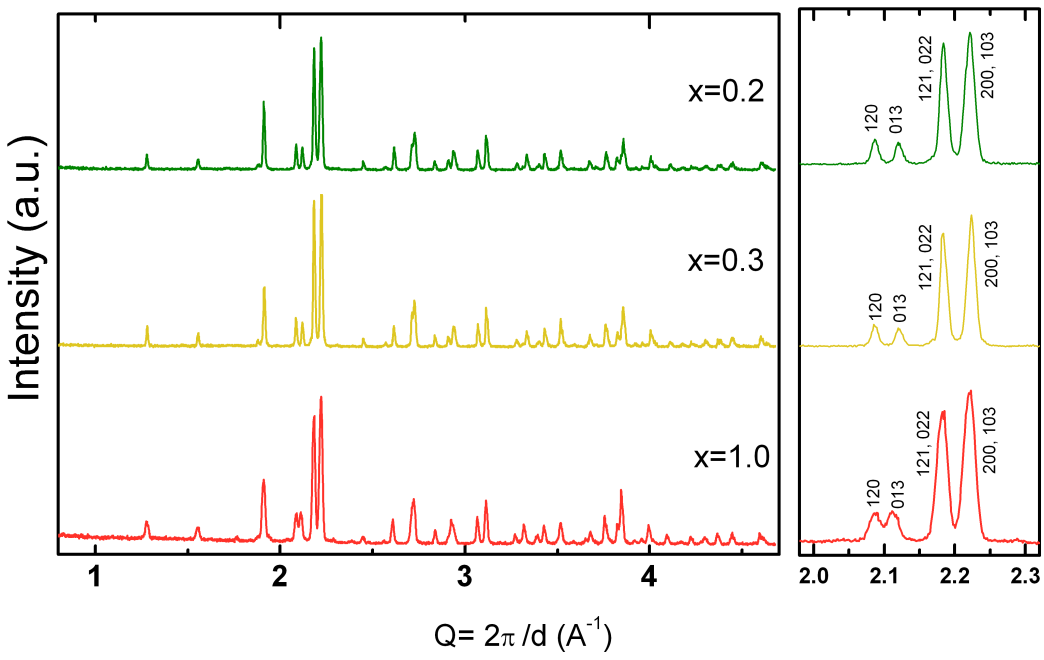


**Figure S2. X-ray powder diffraction patterns for $Sr_{2-x}La_{x-0.02}Ce_{0.02}SiO_{4-x}N_x$ (0.2, 0.3, 1.0) and enlarged images of the intense reflections around Q=2 Å $^{-1}$ region.**

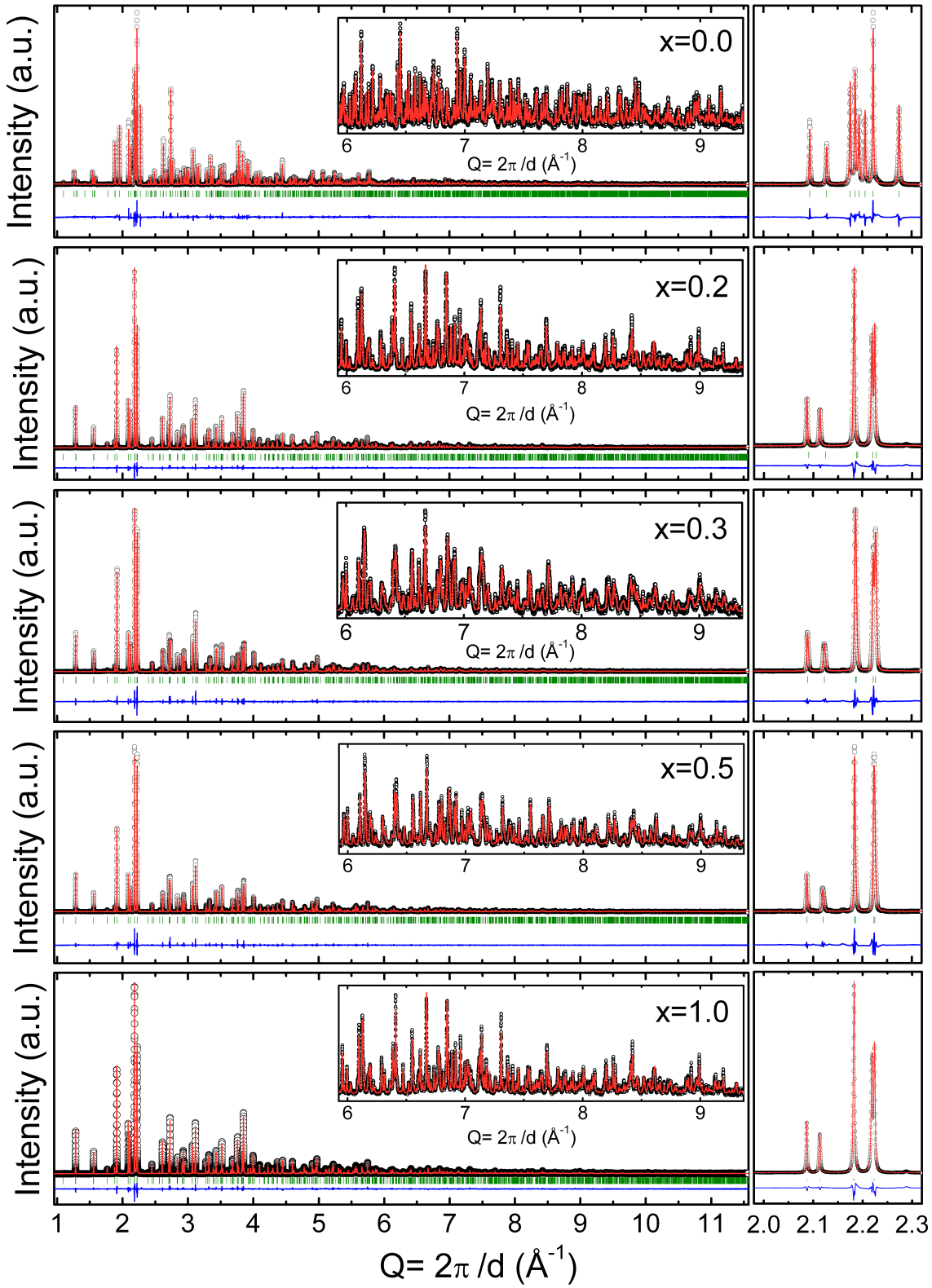


**Figure S3. Observed and calculated synchrotron X-ray powder diffraction patterns for $Sr_{2-x}La_xSiO_{4-x}N_x$.**

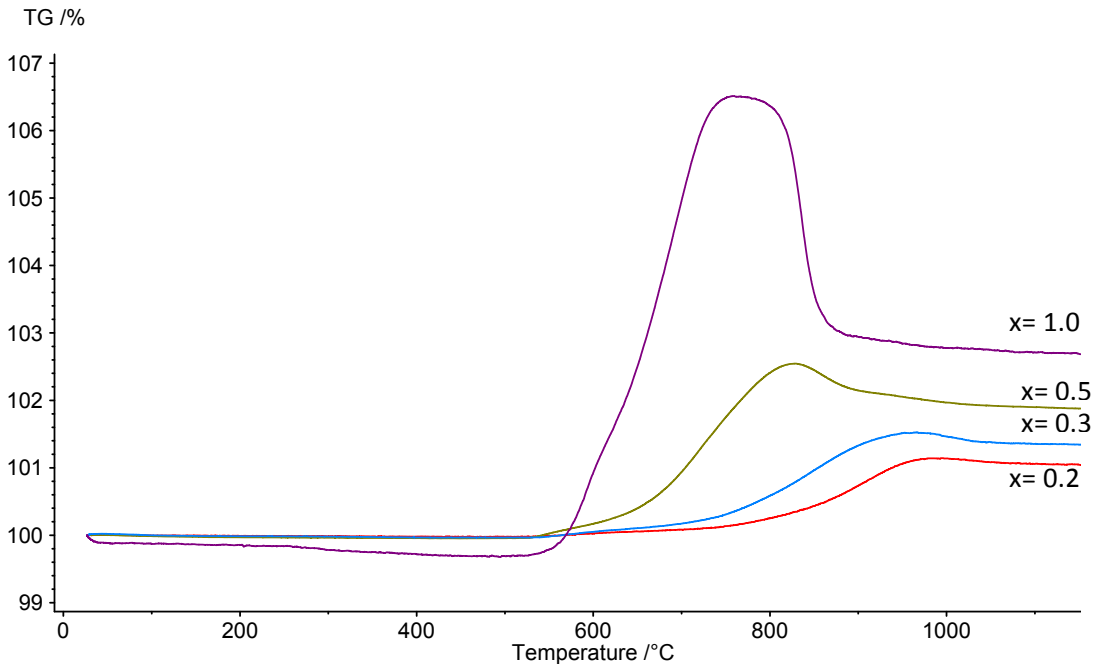


**Figure S4. TGA curves in $O_2$ for $Sr_{2-x}La_xSiO_{4-x}N_x$.**

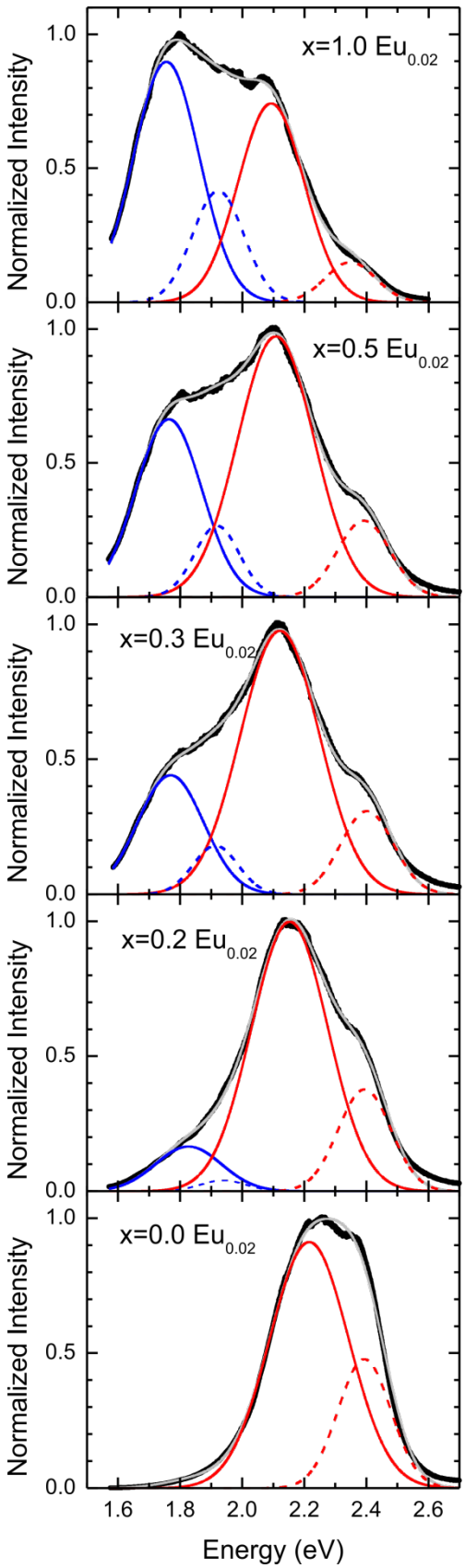


**Figure S5. Deconvolution of emission spectra of $Sr_{2-x}La_xSiO_{4-x}N_x:Eu_{0.02}$ under excitation at 405 nm.**

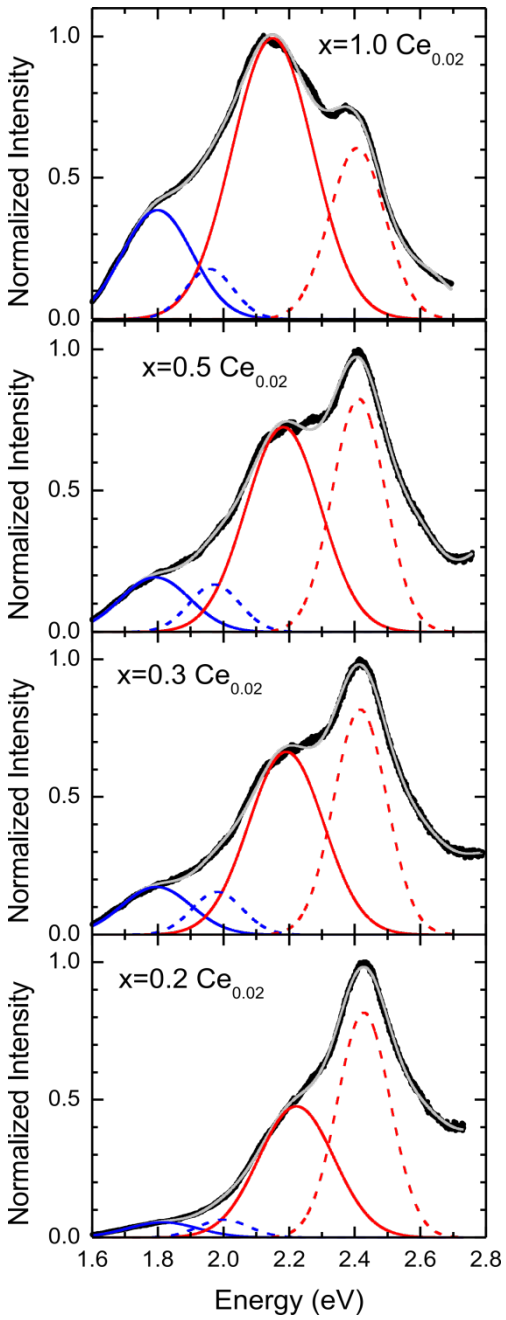


**Figure S6. Deconvolution of emission spectra of $Sr_{2-x}La_xSiO_{4-x}N_x:Ce_{0.02}$ under excitation at 405 nm.**